Journal of Materials Science: Materials in Electronics (2019) 30:2186–2191
https://doi.org/10.1007/s10854-018-0490-2

Effect of nickel (Ni) on the growth rate of Cu_6Sn_5 intermetallic compounds between Sn–Cu–Bi solder and Cu substrate

He Gao[1,2,3] · Fuxiang Wei[1,2,3] · Yanwei Sui[1,2] · Jiqiu Qi[1,3] · Yezeng He[1] · Qingkun Meng[1]

Received: 22 September 2018 / Accepted: 30 November 2018 / Published online: 8 December 2018

Abstract

In this work, the lead-free composite solder was fabricated by mixing Ni element with Sn–0.7Cu–10Bi solder. The effect of nickel (Ni) addition on the growth behavior of intermetallic compounds (IMCs) between Sn–0.7Cu–10Bi–*x*Ni ($x = 0$, 0.05, 0.10, 0.15 and 0.20, in wt%) solder and Cu substrate during the soldering process was studied. The microstructure and the IMCs growth of the solder joints under thermal aging were systematically investigated. The results shown that the addition of Ni element has a slightly influence on melting point of the solder. Moreover, the addition of Ni element can change Cu_6Sn_5 shape from scalloped-like structure into flat-like one. Moreover, the results reveal that Ni can considerably inhibit the growth and reduce the thickness of Cu_6Sn_5. The thickness of Cu_6Sn_5 ranges from 3.07 to 8.42 μm after aging process The diffusion coefficient (D) is 1.80×10^{-3} μm^2 h^{-1} and growth rate (dH/dt) is 4.08×10^{-7} μm s^{-1} of the Cu_6Sn_5 when the Ni content come to 0.15 wt%. The $(Cu,Ni)_6Sn_5$ phase formed in the IMCs layer when Ni was added to the solder, and it can effectively hinder the diffusion of Cu atoms and depressed the growth rate of Cu_6Sn_5.

1 Introduction

The electronics packaging industry has moved toward miniaturization, densification, light weight and high speed, especially in mobile phones, computers and other portable devices [1, 2]. This can result in decreasing the reliability and fatigue life of the solder joints and increasing the current density of components [3, 4]. In the various lead-free solder systems, including Sn–Ag–Cu, Sn–Cu and Sn–Zn solders [5–9], the Sn–0.7Cu solder is widely used in electronic packaging because of its low cost, impurity sensitivity and excellent comprehensive mechanical performance [10, 11], but it is limited in use to some extents due to its high melting point and poor wettability [7, 12, 13]. The melting characteristic is the first and most important property for the new solder alloys, and it determines whether the composite solders can be used in electronic packaging [14]. It is generally recognized that the melting point is close to the melting temperature (183 °C) of the Sn–Pb eutectic point [15]. Too high solder melting point will greatly impact the service life and reliability of electron components, and result in the increase of equipment cost. Zhang et al. found that the addition of Bi could reduce the melting point and improve the wettability of lead-free solder [16, 17], but a high Bi content could lead to poor mechanical properties of solder joints, especially brittle fracture because of inherent brittle nature of Bi [18–21]. Other researchers reported that the comprehensive mechanical properties of solder joints were greatly improved by adding a certain amount of high-melting metal elements such as titanium (Ti), nickel (Ni) and cobalt (Co) to the lead-free solder. With the addition of Ni element, the $(Cu,Ni)_6Sn_5$ phase was formed at the solder joints, the growth of Cu_6Sn_5 was inhibited effectively, and the mechanical properties of joints were improved [20, 22, 23].

It is well known that the interfacial reaction between Cu substrate and solder plays a crucial role in the reliability of solder joints in the service process, and intermetallic compounds (IMCs) formed at the interface during soldering [24]. Cu_6Sn_5 and Cu_3Sn as two most important IMCs

✉ Fuxiang Wei
weifuxiang2001@163.com

1 School of Materials Science & Engineering, China University of Mining & Technology, 1, University Road, Xuzhou 221116, People's Republic of China

2 The Jiangsu Province Engineering Laboratory of High Efficient Energy Storage Technology & Equipments Under, China University of Mining & Technology, Xuzhou, People's Republic of China

3 The Xuzhou City Key Laboratory of High Efficient Energy Storage Technology & Equipments under, China University of Mining & Technology, Xuzhou, People's Republic of China

extremely affected the mechanical properties of solder joints because of the brittle nature of IMCs, and the thicker IMCs will accelerate the brittle failure and reduce the service life of solder joints [25]. During past decades, there were many studies on the kinetics and interfacial reactions of Cu_6Sn_5 IMCs forming between Cu substrate and liquid solder. Li et al. studied the interfacial reaction in the Cu/Sn/Cu system, and reported that the interfacial microstructures and the thickness of the Cu_6Sn_5 layer as well as its growth driving force [26, 27]. In a recent study, Liashenko et al. found the proof of the sequence of Cu_6Sn_5 on the interface between liquid Sn–Cu solder and Cu substrate [28]. To date, however, there is no report on the growth rate of Cu_6Sn_5 layer in the interface reaction and the reduction of melting point of Sn–0.7Cu-X composite solder.

In this study, the Sn–0.7Cu solder was used as a matrix to reduce the melting point by adding a certain amount of Bi element. At the same time, different amount of Ni element was added to improve the mechanical properties of the composite solder. Both average thickness and growth rate of Cu_6Sn_5 are obtained by calculation, and the mechanism of Ni element inhibiting the growth rate of Cu_6Sn_5 is discussed in this paper.

2 Experimental

The Sn–0.7Cu–10Bi–*x*Ni (SCB–*x*Ni, $x = 0$, 0.05, 0.10, 0.15 and 0.20, in wt%) alloy was prepared in a nominal composition, and particles of Sn, Bi, Cu and Ni had a high purity of 99.99%. The master alloy was melted in a vacuum furnace under the high purity argon (Ar) atmosphere. In order to get a homogeneous solder composition the alloy was re-melted four times and then cast into a rod-like model; and the specimens were cut at a diameter of 5 mm and a thickness of 2 mm from the alloy rod. The substrates in this study were commercial copper strips at a dimension of 25 × 25 × 2 mm, and the surface of the Cu substrate was ground down with grit sizes of 400, 600, 1500 and 2000 SiC papers, and cooled in flowing water, then washed with deionized water, cleaned with alcohol and dried at ambient temperature. The specimens were soldered at 230 °C for 250 s, then the solder joints were subjected to the aging at 70 °C for 200 h (h). For micrographic observations, the sample cross-section was cut perpendicular to the Cu substrate and solder interface of the solder joints. The specimens were ground down with 220, 400, 600, 800, 1000, 1200, 1500 and 2000-grit SiC papers, cooled with flowing water, and polished with 0.3 μm and 0.05 μm suspensions of Al_2O_3. In order to remove the residue Al_2O_3 on the surface before etching, the sample was placed in an ultrasonic cleaner with deionized water and methanol, and etched with 4 vol% nitric acid (HNO_3) and 96 vol% alcohol. The IMCs microstructures morphology of the joints was observed using the scanning electron microscope (SEM) equipped with an energy dispersive X-ray spectrometer (EDS). The melting behaviors of SCB–*x*Ni solder alloys were tested via differential scanning calorimetry (DSC). Finally, the IMCs (Cu_6Sn_5) thickness was measured by the Image J software.

3 Results and discussion

3.1 Melting point and microstructure of solder

Figure 1 shows the DSC curves of SCB–*x*Ni solder alloys. The solidus temperature of solder alloys changes slightly with the addition of Ni element. The results show that the new SCB–*x*Ni composite solder has an ideal melting point, and the added Ni exerts a less effect on the melting point of solder. The EDS results of SCB–0.15Ni composite solder analyzed using mapping scanning model are given in Fig. 2. The EDS results reveal that the Sn, Cu, Bi and Ni elements are homogeneously distributed in the solder.

3.2 Microstructure after soldering

In order to distinguish the effect of Ni element on microstructure morphology of interfacial intermetallic compounds (IMCs) between Cu substrate and solder in the aging process, the cross-sectional SEM images of interfacial IMCs were obtained in this study. Figure 3a–e shows the growth of Cu_6Sn_5 in elongated scallop-like IMCs layer after the soldering process. It can be found that almost all scalloped-morphology IMCs are converted to continuous planar-like IMCs after addition of Ni, and the IMCs is short and rod-like when the Ni content is up to 0.20 wt%. The fluctuation of Cu_6Sn_5 layer is not uniform with scallop-like thickness

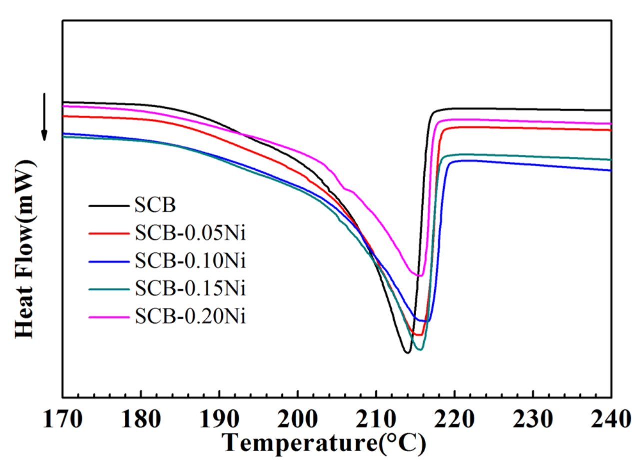

Fig. 1 DSC curves of SCB–*x*Ni solders ($x = 0$, 0.05, 0.10, 0.15 and 0.20, in wt%)

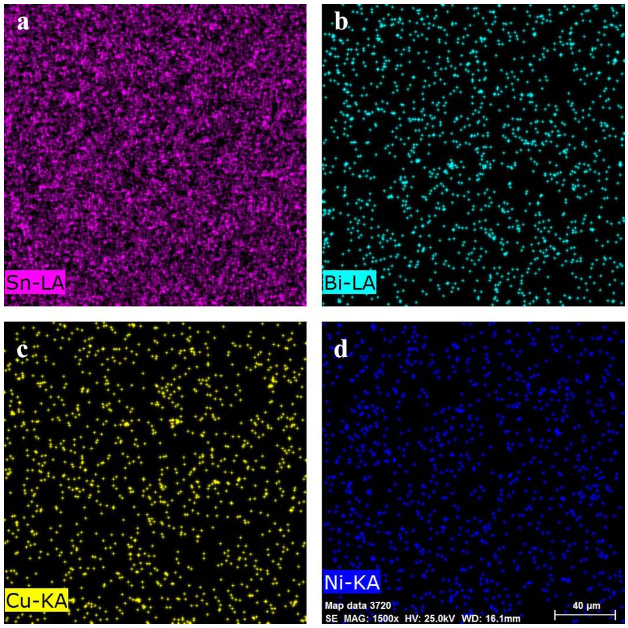

Fig. 2 EDS of elemental mapping for the constituent element: **a** Sn, **b** Bi, **c** Cu and **d** Ni

for non-composite solder/Cu interface. When the Ni content reaches 0.05–0.15 wt%, the Cu_6Sn_5 layer is relatively flat and the scallop-like texture is more refined, presenting a thinner and continuous plane shape of Cu_6Sn_5 layer. The thickness of Cu_6Sn_5 layer continuously increases with the Ni content increasing, and there are small fluctuations near the solder side of Cu_6Sn_5. It can be clearly seen that the IMCs layer of joints mainly consists of Cu_6Sn_5 phase, and the similar results are also founded in the other experiments [29]. Table 1 shows the thickness and other parameters of Cu_6Sn_5 phase between solder and Cu substrate with different Ni content. It is clearly shown that for the addition of 0, 0.05, 0.10, 0.15 and 0.20 wt% Ni element into non-composite SCB solder, the thickness of Cu_6Sn_5 phase (H_1) between solder and Cu substrate in solder joint is 5.40, 4.65, 4.58, 2.47 and 3.53 µm, respectively. This demonstrates that the Ni can effectively hinder the growth of the Cu_6Sn_5 phase. However, when the content of Ni element exceeds 0.15 wt%, the result shows a slightly increase in the thickness of Cu_6Sn_5 phase, which still is thinner than that of non-composite solder joint.

The EDS analyses in spots A and B in Fig. 3i are shown in Fig. 4. Results show that in spot A, the atomic percentage of Ni is 2.97% inside the Cu_6Sn_5 layer. In spot B, the atomic percentage of Ni is 4.62% on the surface of Cu_6Sn_5 layer. The results reveal the existence of Cu_6Sn_5 and $(Cu,Ni)_6Sn_5$ phases in IMCs layer. This coincides with the conclusion in the other literature [13, 25]. The proportion of Ni interface is higher than that of Cu_6Sn_5, indicating that Ni may exist in the form of $(Cu,Ni)_6Sn_5$ phase [30, 31]. The formation of the Cu_6Sn_5 phase is related to Cu atoms concentration in

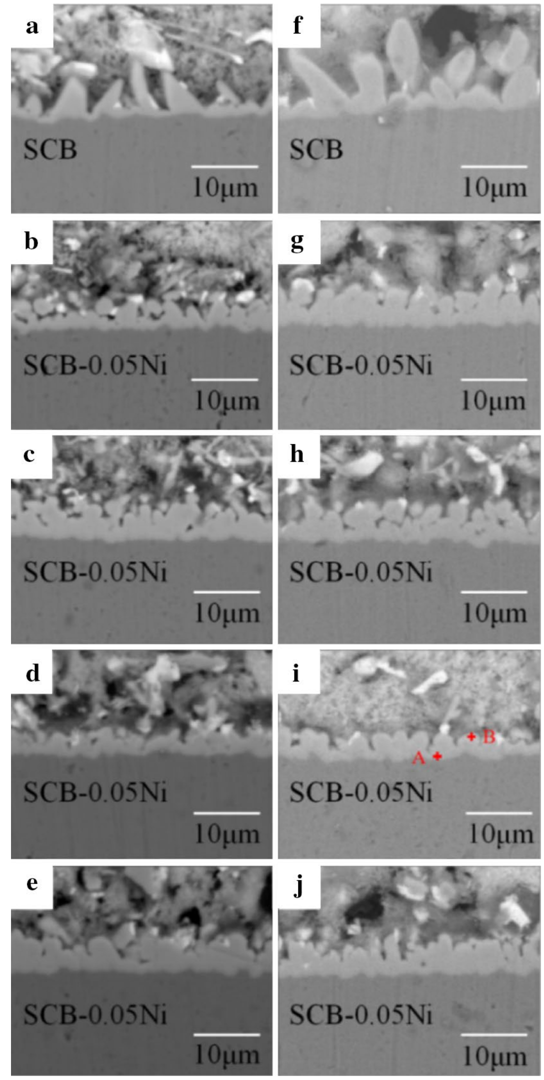

Fig. 3 SEM micrographs of cross-sectional view of SCB–*x*Ni ($x=0$, 0.05, 0.10, 0.15 and 0.20, in wt%) solder joints aging for 0 h: **a** $x=0$, **b** $x=0.05$, **c** $x=0.10$, **d** $x=0.15$ and **e** $x=0.20$; and aging for 200 h at 70 °C: **f** $x=0$, **g** $x=0.05$, **h** $x=0.10$, **i** $x=0.15$ and **j** $x=0.20$

the interface of Cu_6Sn_5/solder, and the Cu_6Sn_5 phase growing into the solder matrix by the consumption of Sn and Cu atoms. The diffusion equilibrium of Cu and Sn atoms will be broken due to the addition of Ni, which can cause the variation and the formation of the new morphology of interfacial Cu_6Sn_5 [20]. When Ni was added to solder as a second phase particle, the solder/Cu interface energy increased in the soldering liquid phase reaction, which inhibited the nucleation and growth process of Cu_6Sn_5. And the $(Cu,Ni)_6Sn_5$ layer in the composite solder joints presented a continuous morphology after soldering process, then the atoms diffusion from the solder to IMCs/solder interface was suppressed. As a result, the growth of IMCs layer declined. The stripe-shape Cu_6Sn_5 layer is formed in the composite solder because

Table 1 Thickness and other parameters of Cu_6Sn_5 phase of SCBi–*x*Ni (*x* = 0, 0.05, 0.10, 0.15 and 0.20, in wt%)

Alloy	T_s (°C)	T_l (°C)	ΔT (°C)	H_1 (μm)	H_2 (μm)	D ($\mu m^2\ h^{-1}$)	dH/dt ($\mu m\ s^{-1}$)
SCB	189.93	214.07	24.14	5.40	8.42	4.56×10^{-2}	6.72×10^{-7}
SCB–0.05Ni	191.26	215.62	24.36	4.65	5.80	6.61×10^{-3}	5.36×10^{-7}
SCB–0.10Ni	191.85	216.50	24.65	4.58	5.48	4.05×10^{-3}	5.03×10^{-7}
SCB–0.15Ni	191.43	215.62	24.19	2.47	3.07	1.80×10^{-3}	4.08×10^{-7}
SCB–0.20Ni	191.26	215.70	24.44	3.53	4.70	6.84×10^{-3}	5.39×10^{-7}

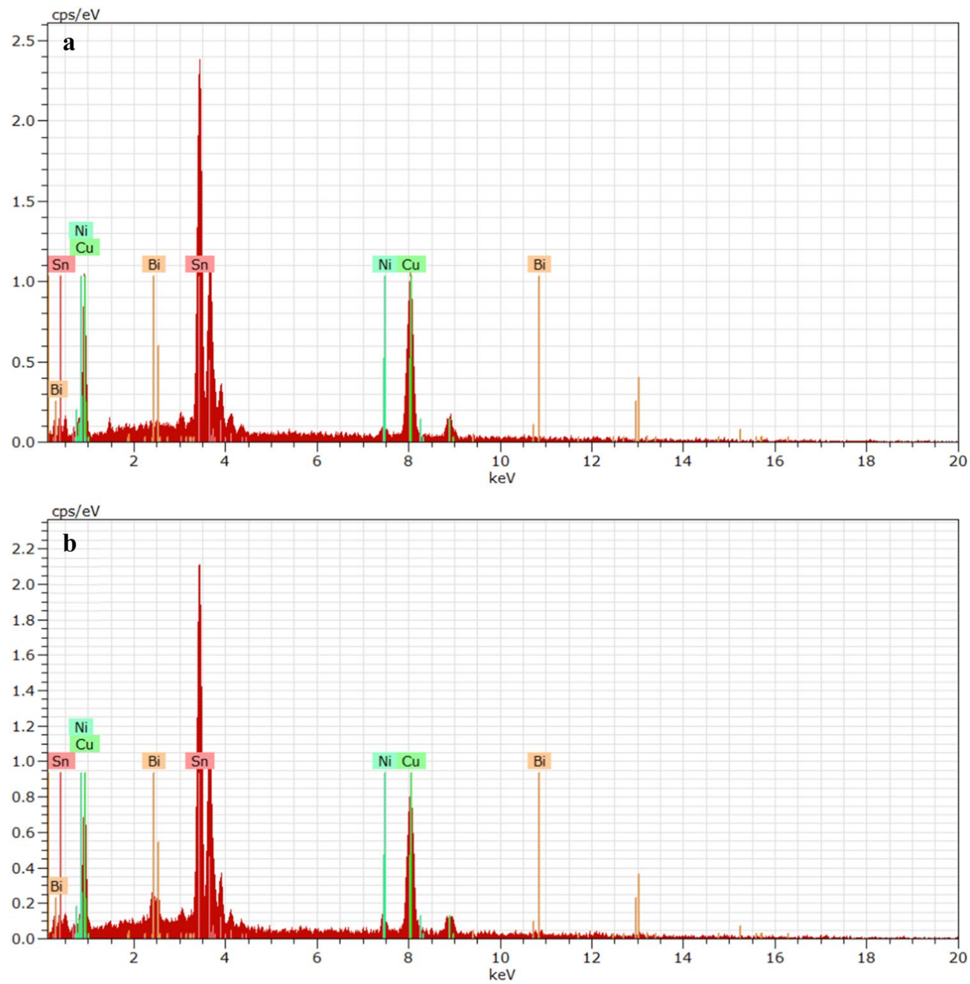

Fig. 4 EDS results for the selected area marked in Fig. 3i **a** and **b**, respectively

the Ni distribution in the Cu/solder interface leads to different diffusion paths of Cu atoms. On the other hand, the $(Cu,Ni)_6Sn_5$ forms in the bulk solder and participates at the interface during solidification. With the addition of Ni, the Cu_6Sn_5 phase became more thermodynamically stable, and the $(Cu,Ni)_6Sn_5$ is also more structurally stable than Cu_6Sn_5 [5, 32]. The diffusion driving force of Cu atoms through $(Cu,Ni)_6Sn_5$ phase is greater than that of Cu_6Sn_5, and this driving force can inhibit the diffusion of Cu atoms from the Cu substrate to the solder [33, 34]. Thus, the concentration of Cu atoms can be decreased and the growth of Cu_6Sn_5 is inhibited, so that the planar shape of Cu_6Sn_5 comes into being and its thickness is reduced.

3.3 Effect of Ni on the growth rate of Cu_6Sn_5

Figure 3 shows the comparison of the IMCs morphology of SCB–*x*Ni (*x* = 0, 0.05, 0.10, 0.15 and 0.20, in wt%) composite solder aging for 0 and 200 h. This indicates that the thickness of Cu_6Sn_5 increases with extension of the aging time. The growth of Cu_6Sn_5 phase can be controlled by inter-diffusion mechanism, and the thickness of the Cu_6Sn_5 layer can be expressed as [31]:

$$X_t = X_0 + \sqrt{Dt} \quad (1)$$

where X_0 is the initial thickness of Cu_6Sn_5, X_t is the thickness of Cu_6Sn_5 at aging time t and D is diffusion coefficient ($\mu m^2\ h^{-1}$). Besides, the difference in the shape of Cu_6Sn_5 is related to flux, and the scallop-shape is controlled by the ripening flux (J_1), while the faceted-shape is mainly caused by the interfacial reaction flux (J_2). The interfacial reaction flux (J_2) and the ripening flux (J_1) can be obtained below [35], respectively.

$$J_1 = \frac{2DM\gamma C_0}{LRT\rho} \times \frac{1}{r^2} \tag{2}$$

$$J_2 = \frac{\rho N_A A v(t)}{2\pi M N_p(t)} \times \frac{1}{r^2} \tag{3}$$

where M is the mole (volume) of Cu_6Sn_5, R is the gas constant, T is the absolute temperature, γ is the interfacial energy between solder and Cu_6Sn_5 of per unit, ρ is the density of pure Cu, r is the radius of Cu_6Sn_5, $N_p(t)$ is the total number of Cu_6Sn_5 grain on the interface of Cu/solder, and $v(t)$ is the consumption rate of Cu substrate.

During aging, the thickness of Cu_6Sn_5 increases in a polynomial trend with addition of Ni at the different amount, as shown in Table 1. Without Ni added into SCB solder, the thickness of Cu_6Sn_5 increases significantly by 55.93%. However, after adding 0.05, 0.10, 0.15 and 0.20 wt% of Ni in the SCB solder, the solder plane increases only by 24.73%, 19.65%, 24.29% and 33.14% respectively. These results can be explained by the $(Cu,Ni)_6Sn_5$ inhibiting the Cu_6Sn_5 growth in the aging process. During this growth, the primary thermodynamic resistance to the Cu_6Sn_5 growth is the increasing interfacial energy between solder and Cu_6Sn_5. The growth rate of Cu_6Sn_5 phase during aging can be written as follows [36]:

$$\frac{dH}{dt} = \frac{D\left(\frac{C_2-C_1}{C_0-C_3}+1\right)}{H(\sqrt{3}H/2\delta+1)} - \frac{C}{C_2-C_1}\frac{DQ^*}{KT^2}\left|\frac{\partial T}{\partial x}\right| \tag{4}$$

where D is the diffusion coefficient of Cu atoms in Cu_6Sn_5 phase, H is the average thickness of the Cu_6Sn_5 phase, C is the dissolved Cu concentration, and C_0, C_1, C_2 and C_3 are the concentrations of the liquid solder near the IMCs interface, Cu_6Sn_5/solder interface, solid Cu_6Sn_5 phase and Cu substrate, respectively. Table 1 shows the calculated results of the growth rate of Cu_6Sn_5 phase during aging for 200 h. Specially, the Cu_6Sn_5 growth rates of SCB, SCB–0.05Ni, SCB–0.10Ni, SCB–0.15Ni and SCB–0.20Ni solder joints are 6.72×10^{-7}, 5.36×10^{-7}, 5.03×10^{-7}, 4.08×10^{-7} and 5.39×10^{-7} $\mu m\ s^{-1}$, respectively. It is seen that the growth rate of Cu_6Sn_5 decreases with Ni added, and the higher growth rate is observed in the case of non-composite solder joints. Moreover, the growth rate of composite solder joints in 0.15 wt% Ni decreases by 39.3% compared with that of SCB solder joint. This trend can be ascribed to the decreasing growth rate of Cu_6Sn_5 with addition of Ni. The addition of Ni element` can suppress the diffusion of Cu atoms from Cu substrate to the solder, and reduce the concentration of Cu atoms at the interface of Cu_6Sn_5/solder. Therefore, this inhibits the growth rate of Cu_6Sn_5. Obviously, the calculated results are consistent with the experimental results, indicating that the addition of Ni can inhibit the growth rate of the Cu_6Sn_5.

4 Conclusions

In summary, the effect of Ni element on Cu_6Sn_5 growth in Sn–0.7Cu–10Bi-*x* wt% Ni solder joints in isothermal aging process has been studied in this study. When the content of Ni is up to 0.15 wt%, the Cu_6Sn_5 layer presents a lower growth rate (dH/dt) of 4.08×10^{-7} $\mu m\ s^{-1}$, a smallest diffusion coefficient (D) of 1.80×10^{-3} $\mu m^2\ h^{-1}$ and a thinner thickness (H_2) of 3.07 μm under isothermal aging for 200 h. In addition, a new phase $(Cu,Ni)_6Sn_5$ forms in the IMCs layer when Ni is added to the solder. $(Cu,Ni)_6Sn_5$ can effectively prevent the diffusion from Cu substrate to solder and reduce Cu_6Sn_5 interface concentration of Cu atoms. Thus, the growth rate of Cu_6Sn_5 phase is reduced and the thickness of IMCs layer is restricted.

Acknowledgements This work was supported by the Fundamental Research Funds for the Central Universities (2017XKQY004).

References

1. Y.C. Chan, D. Yang, Prog. Mater. Sci. **55**, 428–475 (2010)
2. H.Y. Lee, A. Sharma, S.H. Kee, Y.W. Lee, J.T. Moon, J.P. Jung, Electron. Mater. Lett. **10**, 997–1004 (2014)
3. Z.L. Ma, S.A. Belyakov, K. Sweatman, T. Nishimura, T. Nishimura, C.M. Gourlay, Nat. Commun. **8**, 1916 (2017)
4. A. Sharma, D.H. Jung, M.H. Roh, J.P. Jung, Electron. Mater. Lett. **12**, 1–8 (2016)
5. K. Nogita, Intermetallics **18**, 145–149 (2010)
6. A. Sharma, D.E. Xu, J. Chow, M. Mayer, H.R. Sohn, J.P. Jung, Electron. Mater. Lett. **11**, 1072–1077 (2015)
7. P. Xue, S.B. Xue, Y.F. Shen, F. Long, H. Zhu, J. Mater. Sci. Mater. Electron. **25**, 3520–3525 (2014)
8. X. Long, W. Tang, S. Wang, X. He, Y. Yao, J. Mater. Sci. Mater. Electron. **29**, 7177–7187 (2018)
9. A.A. El-Daly, A. Fawzy, S.F. Mansour et al., J. Mater. Sci. Mater. Electron. **24**, 2976–2988 (2013)
10. A.A. El-Daly, A.E. Hammad, Mater. Des. **40**, 292–298 (2012)
11. M.A.A.M. Salleh, A.M.M.A. Bakri, M.H. Zan Hazizi, F. Somidin, N.F.M. Alui, Z.A. Ahmad, Mater. Sci. Eng. A **556**, 633–637 (2012)
12. C.M. Gourlay, K. Nogita, A.K. Dahle et al., Acta Mater. **59**, 4043–4054 (2011)
13. Satyanarayan, K.N. Prabhu, Adv. Colloid Interface Sci. **166**, 87 (2011)

14. M.E. Alam, M. Gupta, Electron. Mater. Lett. **10**, 515–524 (2014)
15. C. Morando, O. Fornaro, O. Garbellini, H. Palacio, J. Mater. Sci. Mater. Electron. **25**, 3440–3447 (2014)
16. L. Yang, C. Du, J. Dai et al., J. Mater. Sci. Mater. Electron. **24**, 4180–4185 (2013)
17. F. Wang, H. Chen, Y. Huang, C. Yan, J. Mater. Sci. Mater. Electron. **28**, 1–12 (2018)
18. Z. Lai, D. Ye, J. Mater. Sci. Mater. Electron. **27**, 3182–3192 (2016)
19. X.P. Zhang, C.B. Yu, Y.P. Zhang, S. Shrestha, L. Dorn, J. Mater. Process. Technol. **192**, 539–542 (2007)
20. K. Kanlayasiri, T. Ariga, Mater. Des. **86**, 371–378 (2015)
21. Y. Ma, X. Li, W. Zhou, L. Yang, P. Wu, Mater. Des. **113**, 264–272 (2017)
22. T. Laurila, V. Vuorinen, M. Paulasto-Kröckel, Mater. Sci. Eng. R **68**, 1–38 (2010)
23. Q.B. Tao, L. Benabou, L. Vivet, V.N. Le, F.B. Ouezdou, Mater. Sci. Eng. A **669**, 403–416 (2016)
24. Y.-K. Lee, Y.H. Ko, J.K. Kim et al., Electron. Mater. Lett. **9**, 31–39 (2013)
25. T. Laurila, V. Vuorinen, J.K. Kivilahti, Mater. Sci. Eng. R **37**, 1–60 (2006)
26. J.F. Li, P.A. Agyakwa, C.M. Johnson, Acta Mater. **59**, 1198–1211 (2011)
27. J.F. Li, S.H. Mannan, M.P. Clode, D.C. Whalley, D.A. Hutt, Acta Mater. **54**, 2907–2922 (2006)
28. O.Y. Liashenko, S. Lay, F. Hodaj, Acta Mater. **117**, 216–227 (2016)
29. H. Ji, Y. Qiao, M. Li, Scr. Mater. **110**, 19–23 (2016)
30. G. Ban, F. Sun, Y. Liu, S. Cong, Solder. Surf. Mt. Technol. **29**, 92–98 (2017)
31. P.L. Tu, Y.C. Chan, K.C. Hung, J.K.L. Lai, Scr. Mater. **44**, 317–323 (2001)
32. F. Gao, T. Takemoto, H. Nishikawa, Mater. Sci. Eng. A **420**, 39–46 (2006)
33. A.A. El-Daly, A.M. El-Taher, T.R. Dalloul, Mater. Des. **55**, 309–318 (2014)
34. K. Nogita, T. Nishimura, Scr. Mater. **59**, 191–194 (2008)
35. H.F. Zou, H.J. Yang, Z.F. Zhang, Acta Mater. **56**, 2649–2662 (2008)
36. N. Zhao, Y. Zhong, M.L. Huang, H.T. Ma, W. Dong, Sci. Rep. **5**, 13491 (2015)